Helicity fluctuations and turbulent energy production in rotating and non-rotating pipes

By P. Orlandi[1]

1. Motivation and objectives

In this paper finite-difference second-order accurate direct simulations have been used to investigate how the helicity density fluctuations change when a turbulent pipe rotates about its axis. In this case the rotation axis is in the direction of the near wall vortical structures, which play a fundamental role on the wall friction and turbulence production. The helicity density is the trace of the tensor $\gamma'_{ij} = <v'_i\omega'_j>$ whose elements form the components of $\mathbf{v}' \times \boldsymbol{\omega}'$. When the momentum equations are written in rotational form, the turbulence energy production splits into two parts, one related to the convection of the large scales and the other related to the energy cascade to the small scales. From data of direct simulations the modifications of the turbulent energy production in different regions of the pipe have been analyzed by finding the *pdf* of the components of $\mathbf{v}' \times \boldsymbol{\omega}'$ and by their connection to the modifications of the vortical structures. The joint *pdf* of the dissipation with the helicity density has shown that the dissipation is highly correlated with regions of very low helicity density in the non-rotating pipe. When the pipe rotates the helicity density increases and the dissipation decreases, since in this case there is a drag reduction. It has been speculated that the alignment between velocity and vorticity could be a common feature in drag reducing flows.

The turbulent pipe rotating about its axis is important for many engineering applications such as rotating heat exchangers and cooling systems of rotors, but it is also interesting since it is a configuration where the external rotation is oriented in the same direction as the near wall vortical structures. Recently there is a wide consensus that the streamwise vortical structures are responsible for the wall friction and for the turbulence production. Therefore the control of wall turbulence by acting on these structures should be further pursued. A possible action could be the imposition of a background rotation. Bardina *et al.* (1985) observed that in isotropic turbulence the background rotation reduced the energy transfer to the small scales. In inhomogeneous flows the rotation was applied in the same direction as the main vorticity, e.g. Kim (1983) performed the direct simulation of a plain channel rotating about the streamwise direction and Metais *et al.* (1995) of a mixing layer with the rotation parallel to the vorticity of the rolls. In planar flows, with periodicity in the spanwise direction, it is difficult to imagine an experiment with the rotation axis parallel to the direction of the secondary vortical structures. On

1 Università di Roma "La Sapienza" Dipartimento di Meccanica e Aeronautica, via Eudossiana 18 00184 Roma, Italy.

the contrary, in a turbulent pipe or in a round jet the application of the background rotation with the same orientation as the secondary vortical structures is feasible in a numerical as well as in a real experiment. In the present paper we are thus studying a pipe rotating around its axis.

The most important outcome of the rotating pipe is a drag reduction that increases with the rotation rate, as it was experimentally observed by Nishibori *et al.* (1987) and Reich & Beer (1989) and numerically by Orlandi & Fatica (1995). In the numerical simulation it was shown that the drag reduction is caused by a change in the structure of the near wall vorticity. In the direct simulation, instead of a rotating wall, a reference frame moving with the wall has been used and a Coriolis body force appears. This choice allows us to see from the equation of motion how each component of the turbulent stress is affected by the rotation. In the present paper as well as in the previous one (Orlandi & Fatica 1995) the aim is to reach a clear comprehension of the causes of drag reduction in a rotating pipe that could be useful in finding the most effective way to achieve wall turbulence control. In previous simulations in a straight channel, for example, it was observed that spanwise pressure gradients (Sendstadt & Moin, 1993) produced drag reduction. The rotating pipe presents analogies with this configuration.

In the present paper we analyze the tensor $\gamma_{ij} = < v_i \omega_j >$ which appears in the vorticity as well as in the momentum equation. The averages $<>$ are performed in the two homogeneous directions over a large number of fields separated by three non-dimensional time units. Often it is objected that the γ_{ij} tensor of the instantaneous fields is not Galilean invariant. To overcome this criticism we considered only the tensor γ'_{ij} of the fluctuating quantities. The trace of the tensor is the helicity density, and the other elements give the three components of the $\mathbf{v}' \times \boldsymbol{\omega}'$ vector. Hussain (1986) as well as Rogers and Moin (1987) observed from the identity $|\mathbf{v}' \times \boldsymbol{\omega}'|^2 + |\mathbf{v}' \cdot \boldsymbol{\omega}'|^2 = |\mathbf{v}'|^2 |\boldsymbol{\omega}'|^2$ that since the term $|\mathbf{v}' \times \boldsymbol{\omega}'|^2$ indicates a high rate of energy cascade to smaller scales, it might be expected that regions of high helicity density are regions where the energy cascade is inhibited. Rogers & Moin (1987) focused their attention on isotropic, homogeneous turbulence as well as on the channel. For the channel they got different results from those of Pelz *et al.* (1985) and they affirmed that it is questionable whether helicity fluctuations play an important role in three-dimensional incompressible turbulence in complete disagreement with the Pelz *et al.* conclusions. Since a similar pseudospectral numerical method was used in the two studies but with different resolution, we have made a further study of the turbulent pipe to provide a further check on the importance of the helicity density in turbulent wall flows. The same calculations have been performed recently by Tsinober *et al.* (1995) through a data base generated by a numerical method with a resolution similar to the present one. As expected, the pipe results agree with those of Rogers & Moin (1987) for the channel. Tsinober *et al.* (1995) further focused the study on the alignment between vorticity and vortex stretching and the vorticity and the rate of strain tensor. However, they did not investigate the properties of $\mathbf{v}' \times \boldsymbol{\omega}'$, which have been analyzed here.

The comparative analysis performed in this study between the helicity fluctuations in the non-rotating and rotating pipe show that this quantity could have a relevance in the detection of conditions leading to drag reduction.

2. Accomplishments

Orlandi & Fatica (1995) have shown that the second and higher order statistics of the velocity field for the non-rotating pipe agreed with those obtained in other simulations (Eggels *et al.* (1994)) as well as in experiments at the same low Reynolds number. In the rotating case $N = V_{\theta 0}/U_b$ indicates the ratio between the bulk velocity U_b and the rotation velocity of the wall $V_{\theta 0}$. The dimensionless number N is the inverse of the Rossby number $Ro = U_P/2\Omega R$, usually used in geophysical flows, where Ω is the background rotation, U_P is the laminar pipe Poiseuille centerline velocity, and R is the radius of the pipe (R=1). The Reynolds number based on the radius R and U_P in the present simulation was set equal to 4900, which gives a Reynolds number based on the friction velocity, $Re_\tau = 172.4$ for $N = 0$ and $Re_\tau = 156.9$ for $N = 2$. In a previous paper of Orlandi & Fatica (1995), a comparison was made for $N = 0, 0.5, 1, 2$, with the mean velocity profiles of Reich & Beer (1989) since Nishibori *et al.* (1987) showed that the turbulence profiles largely depend on the inlet conditions. However, the grid independence for the *rms* velocity was checked by increasing the number of points in the radial and axial directions. Since here the interest is directed to investigate quantities related to the vorticity field, the present *rms* vorticity has been compared with that by Kim *et al.* (1987) in the channel. Fig. 1a shows that the present numerical method predicts profiles very similar to those in the channel. By grid refinement it has been checked that the differences in Fig. 1a are not related to insufficient grid resolution. From Fig. 1a we see the numerical method is accurate, in agreement with Choi *et al.* (1991), who claim that the vorticity *rms* is a good indicator of the accuracy of a numerical scheme. In the pseudospectral simulations the velocity and the vorticity are evaluated at the same physical positions. On the contrary in the present scheme, velocity and vorticity components are evaluated at different points of the cell, leading to further truncation errors in the evaluation of the statistics at the cell center.

At the rotation rate $N = 2$ Fig. 1b shows that in the wall region there are substantial modifications of the *rms* vorticity profiles. Orlandi & Fatica (1995) through numerical flow visualizations have shown that the substantial reduction of ω'_r is responsible for the reduction in intensity of the low and high speed streaks. Contour plots emphasized that in the non-rotating case contour levels of ω'_r are directed in the streamwise direction, whereas in the rotating pipe these are inclined and their magnitude is reduced. A similar effect was observed by Sendstadt & Moin (1992) in the simulation of a three-dimensional boundary layer.

In the non-rotating case the mean profiles of the fluctuating helicity components $< h_\theta >, < h_r >, < h_x >$ defined as $< v_\theta \omega'_\theta >, < v'_r \omega'_r >, < v'_x \omega'_x >$ have very small amplitudes (Fig. 2b), and this indicates that there is an equal probability of right- or left-handed helical motions within the turbulent field. When the mean rotation is
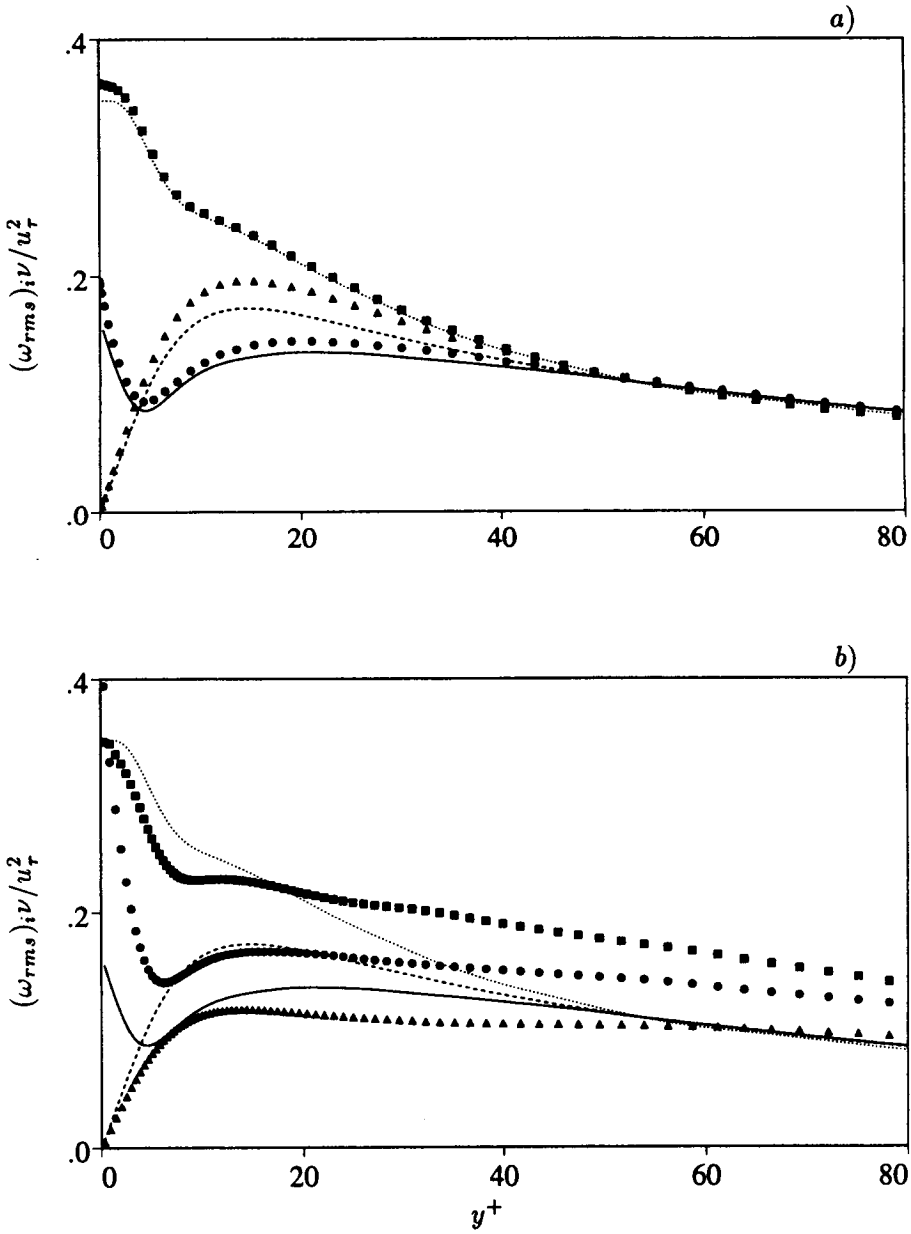
P. Orlandi

FIGURE 1. Profiles of *rms* vorticity fluctuations, a) lines, pipe. Symbols, channel by Kim *et al.*, b) lines $N = 0$, symbols $N = 2$; (——— and $\bullet$ ω'_x), (– – – – and $\triangle$ ω'_r), (········· and $\blacksquare$ ω'_θ).

a)

b)

FIGURE 2.   Profiles of a) *rms* velocity fluctuations, (——— and ● v'_x), (– – – – and △ v'_r), (········· and ■ v'_θ), b) helicity density, (——— and ● $\omega'_x v'_x$), (– – – – and △ $\omega'_r v'_r$), (········· and ■ $\omega'_\theta v'_\theta$); lines $N = 0$, symbols $N = 2$.
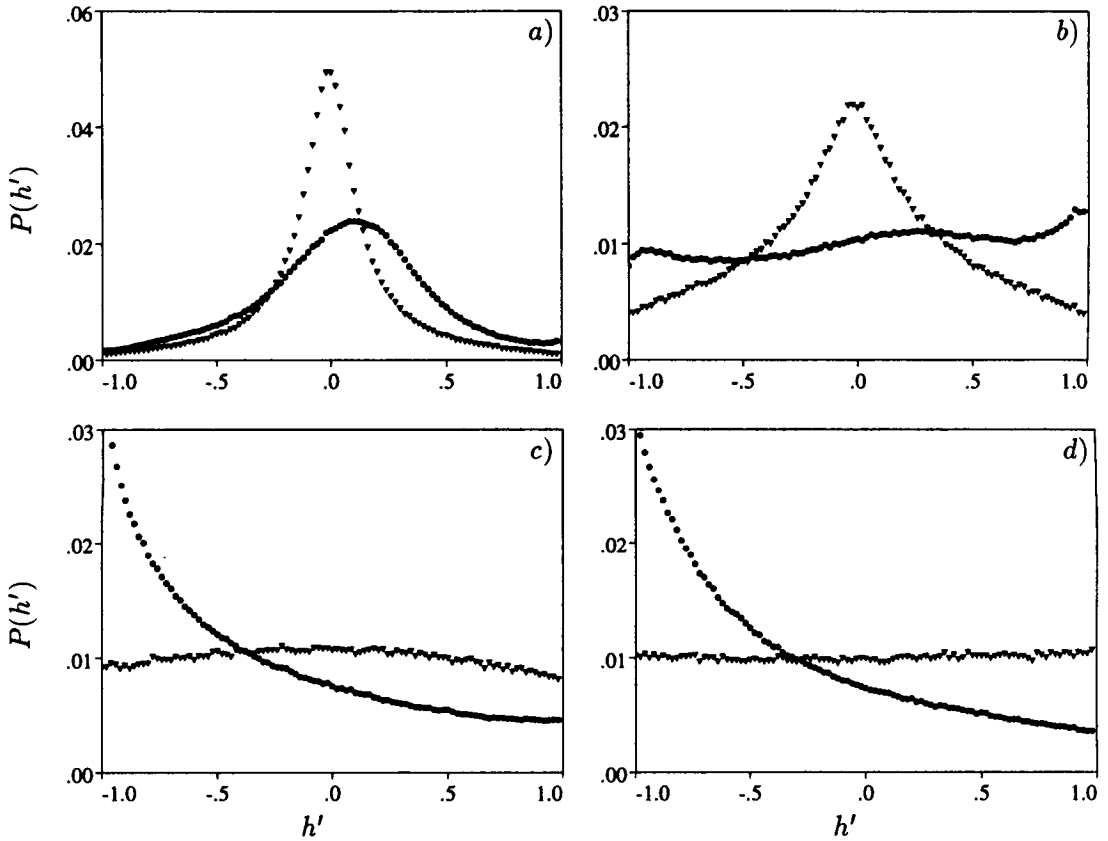
FIGURE 3.   Probability density function of the helicity density, a) $y^+ = 4$, b) $y^+ = 10$, c) $y^+ = 50$, d) $y^+ = 120$; $\triangle$ $N = 0$, $\bullet$ $N = 2$.

applied, the profiles changes everywhere in the pipe. Since the rotation is breaking the symmetry between right- and left-handed helical structures, the *pdf* of the angle between the velocity and vorticity fluctuations ($h' = \mathbf{v}' \cdot \boldsymbol{\omega}'/\sqrt{|\mathbf{v}|^2|\omega|^2}$) is a useful tool to understand the changes in Fig. 2b.

Fig. 3b shows, as found by Rogers & Moin (1987) in the channel, that at $y^+ = 10$, the position of maximum energy production, the vorticity and the velocity fluctuations are not aligned. This poor alignment is due to the fact that in the wall region, as shown in Fig. 1a, ω'_θ is the greatest component and from Fig. 2a that v'_x is greater than the other two components. The nonalignment increases as the wall is approached, see Fig. 3a, and in the log region the *pdf* is relatively flat as in isotropic turbulence (see Figs. 3c-d). When the rotation is imposed the nonalignment persists in the viscous region (Fig. 3a), but the loss of symmetry causes the large variations of the helicity density shown in Fig. 2b. From the *pdf* of each component, not shown here, we find that the rotation produces a positive angle between the azimuthal components. In the streamwise direction, on the contrary, there is a large probability that the low speed streaks ($v'_x < 0$) are correlated
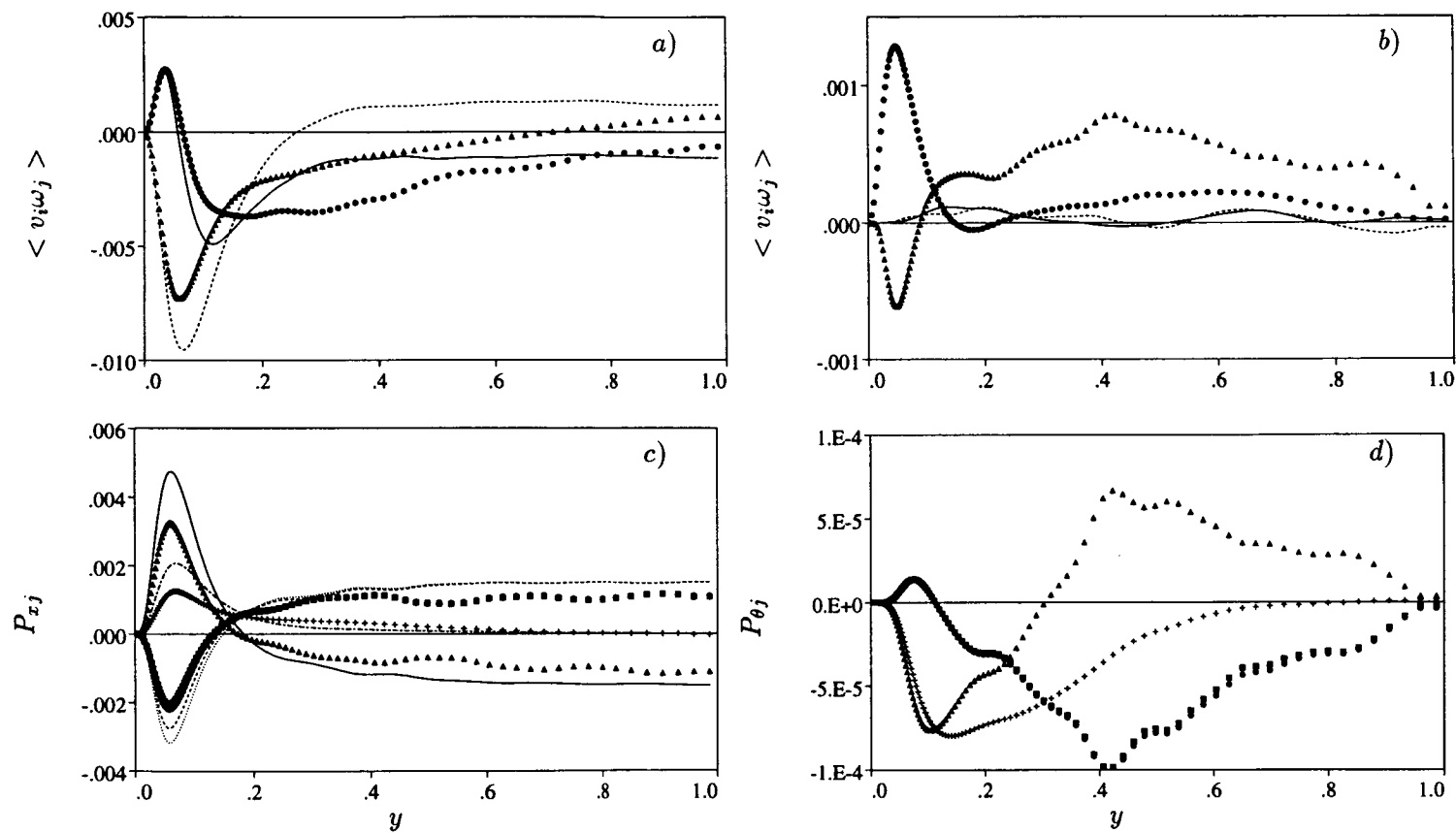
FIGURE 4.   Profiles of a) (——— and ● $< \omega'_\theta v'_r >$), (- - - - and △ $< \omega'_r v'_\theta >$); b) (——— and ● $< \omega'_r v'_x >$), (- - - - and △ $< \omega'_x v'_r >$); c) (——— and △ P_{xC}), (- - - - and ● P_{xR}), (········ and ■ P_{xI}), (— · — + $P_{xR} - P_{xC}$);d) (——— and △ $P_{\theta C}$), (- - - - and ● $P_{\theta R}$), (········ and ■ $P_{\theta I}$), (— · — + $P_{\theta R} - P_{\theta C}$); lines $N = 0$, symbols $N = 2$.

with positive ω_x' and vice-versa. Fig. 3b shows that in the region of maximum turbulent energy production, the rotation produces a strong alignment between the fluctuating velocity and vorticity. This increase of the alignment with rotation is due to the increase of ω_x' and of v_θ'. However the almost equal probability of alignment and counteralignment explains why in Fig. 2b at $y \approx 0.5$ two helicity components intersect the axis. For $y < 0.5$ there is an alignment, and it produces positive values of the helicity density in Fig. 2b; on the other hand in the central region of the pipe, the counteralignment explains the negative values in Fig. 2b. This alignment between velocity and vorticity fluctuations in the near wall region can then be considered as an indication of the drag reduction. In the central region the non zero helicity density is an indication of the energy transfer reduction leading to the increase of the turbulent energy as shown in Fig. 2a. From the *pdf* of each of the helicity components, not reported here, it is shown that the alignment and the counteralignment at $y^+ = 10$ (Fig. 3b) are due to the θ and x components with the θ contribution being the more important. This condition is caused by the increase of the *rms* values of v_θ' and decrease of v_x'. The total kinetic energy in the rotating case decreases near the wall and increases in the central region. It is therefore interesting to investigate the reasons for the changes in the turbulent energy production and dissipation.

Since the production of turbulent energy can be linked to $\mathbf{v}' \times \boldsymbol{\omega}'$, it is interesting to look at the distribution of each term across the pipe. When the convective terms of the Navier-Stokes equations are written in the rotational form, the production terms of turbulent kinetic energy are

$$
\begin{aligned}
&-U_x[< v_\theta'\omega_r' > - < \omega_\theta'v_r' >] + \frac{1}{r}\frac{\partial r U_x < v_x'v_r' >}{\partial r} + \\
&-U_\theta[< v_r'\omega_x' > - < \omega_r'v_x' >] + \frac{1}{r}\frac{\partial r U_\theta < v_\theta'v_r' >}{\partial r} + \\
&-U_r[< v_x'\omega_\theta' > - < \omega_x'v_\theta' >] + \frac{1}{r}\frac{\partial r U_r < v_r'v_r' >}{\partial r}.
\end{aligned}
\tag{1}
$$

These six terms for brevity can be indicated respectively by P_{xR}, P_{xC}, $P_{\theta R}$, $P_{\theta C}$, P_{rR}, P_{rC}; the terms P_{rR} and P_{rC} have been left in Eq. (1) although both in the rotating and in the non-rotating case $U_r = 0$. The other observation is that in the rotating case, at least at this intermediate rotation rate ($N = 2$), U_θ is much smaller than U_x. To understand the effect of the external rotation in the wall region, the plots of the radial profiles of axial and azimuthal components of $< \mathbf{v}' \times \boldsymbol{\omega}' >$ are shown in Figs. 4a-b. Since the following identities hold:

$$
\begin{aligned}
U_x[< v_\theta'\omega_r' > - < \omega_\theta'v_r' >] &= \frac{U_x}{r}\frac{\partial r < v_x'v_r' >}{\partial r} = P_{xI}, \\
U_\theta[< v_r'\omega_x' > - < \omega_r'v_x' >] &= \frac{U_\theta}{r^2}\frac{\partial r^2 < v_\theta'v_r' >}{\partial r} = P_{\theta I}.
\end{aligned}
\tag{2}
$$

the right-hand sides have been also plotted in Fig. 4c, where, as found by Tsinober *et al.* (1995), in the simulation the identities do not hold. The reason for the unbalance

is related to the interpolations needed to evaluate each term of $< \mathbf{v}' \times \boldsymbol{\omega}' >$. In our scheme we were not able to find a discretization scheme preserving exactly the identity. In the rotating case the unbalance is reduced, and this circumstance confirms that the distributions of fluctuating velocity and vorticity components are smoother and that interpolation errors are reduced.

Before describing the effects of the external rotation on the $\mathbf{v}' \times \boldsymbol{\omega}'$ terms, and the *pdf* of the components of the vector $\mathbf{p}' = \mathbf{v}' \times \boldsymbol{\omega}'/\sqrt{|\mathbf{v}'|^2|\boldsymbol{\omega}'|^2}$), it is interesting to analyze the meaning of the terms in Eq. (1). For $N = 0$ the turbulent energy production is given only by the first two terms in Eq. (1). The first term is related, as asserted by Rogers & Moin (1987), to the cascade of energy from large to small scales, showing energy is lost or gained depending on the radial position. Near the wall energy is lost; in contrast, in the central region energy is gained. The difference between the first and the second term in Eq. (1) gives the turbulent energy production, which is positive everywhere. Both in the rotating and in the non-rotating case the first two terms give the major contribution to the turbulence energy production as shown in Fig. 4c-d. The radial component of $\mathbf{v}' \times \boldsymbol{\omega}'$ (not shown here) is the greatest, but since it is multiplied by U_r in both cases, it gives a null contribution to the turbulence production. On the contrary, when the external rotation is applied, the θ component increases (Fig. 4b), and since it is multiplied by U_θ, it gives a contribution smaller (Fig. 4d) than that in the x direction, which is multiplied by U_x (Fig. 4c). In the rotating case, the axial component is reduced at $y^+ = 10$ (Fig. 4c) with $< v'_\theta \omega'_r >$ decreasing more than $< v'_r \omega'_\theta >$. Since v'_θ does not have a large variation, the reduction is mainly due to the *rms* value of ω'_r. This reduction, as before mentioned, is due to the changes of orientation, spacing, and size of the vortical structures near the wall.

Figs. 5a-d show the *pdf* of the three components of $\mathbf{v}' \times \boldsymbol{\omega}'$ at the same positions where the *pdf* of the helicity density were given in Fig. 3. The first consideration is that near the wall the vector $\mathbf{v}' \times \boldsymbol{\omega}'$ is counteraligned with the r direction; that is, it is pointing out from the wall. This orientation is maintained also when the pipe rotates. Near the wall, Fig. 4a shows that $| < v'_r \omega'_\theta > | > | < v'_\theta \omega'_r > |$, and from Figs. 5a-b the positive contribution of $< v'_r \omega'_\theta > - < v'_\theta \omega'_r >$ is due to the ejection and sweep events producing the higher correlations of v'_θ and ω'_r of same sign. Figs. 5a-b, moreover, confirm that near the wall the radial component of $\mathbf{v}' \times \boldsymbol{\omega}'$ is the greatest and that it is weakly influenced by the rotation. However, even if the vortex dynamics could change the radial distribution of $< v'_x \omega'_\theta > - < v'_\theta \omega'_x >$, its contribution to the energy production is null. Near the wall the rotation breaks the symmetry of the $< v'_x \omega'_r > - < v'_r \omega'_x >$, and this term becomes negative as shown in Figs. 5a-b where the contribution to the θ component is due to the correlation of opposite sign between v'_r and ω'_x. In the inner part of the pipe there is no preferred orientation between fluctuating velocity and vorticity, which is the condition characteristic of weak turbulence production. In this region Fig. 4c shows in the non-rotating case that the amount of turbulent energy production due to $\mathbf{v}' \times \boldsymbol{\omega}'$ is positive and it is balanced by the energy convected from the large scales. Fig. 5c shows that this positive contribution is due to the greater probability of
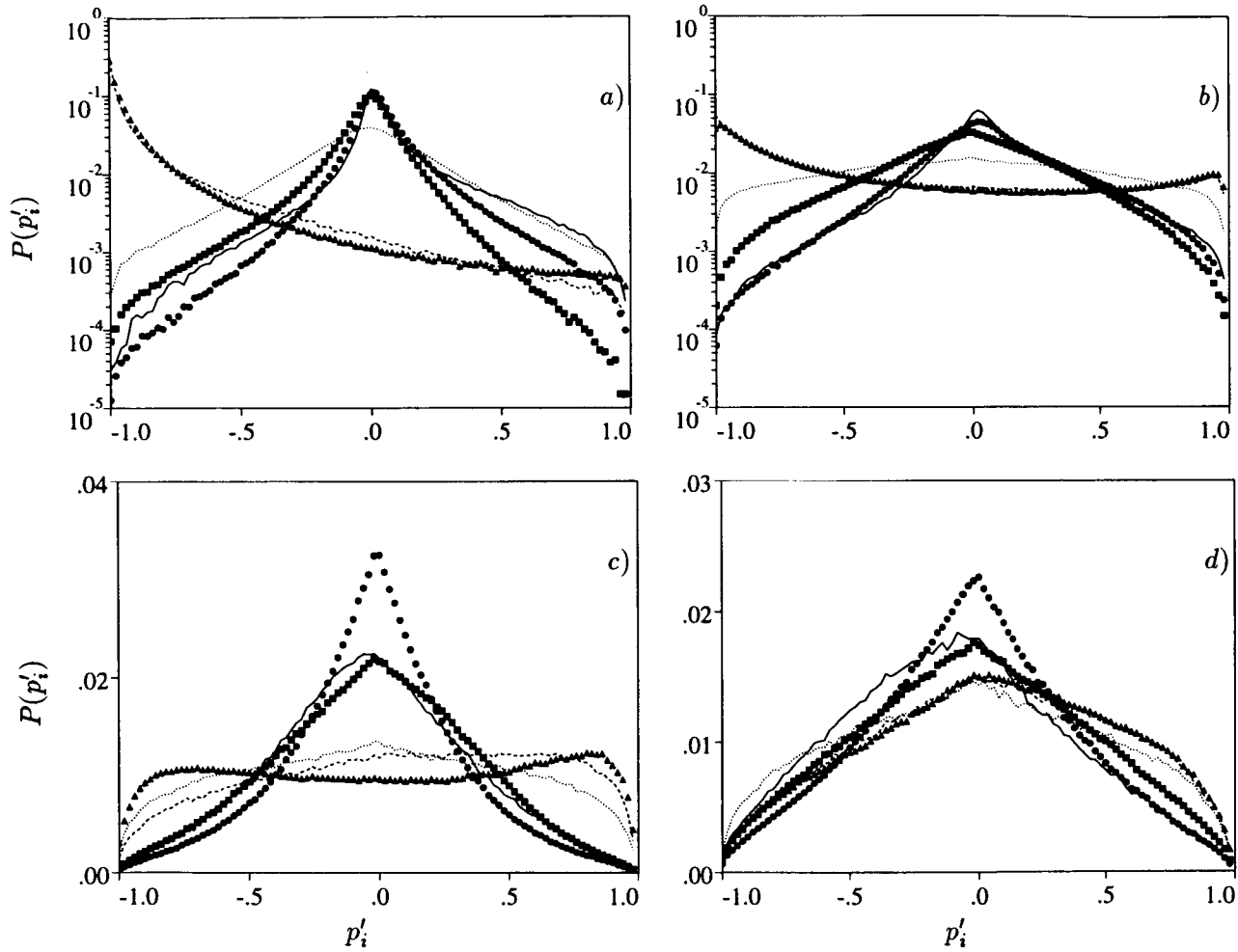
FIGURE 5. Probability density function of (——— and ● p'_x), (- - - - and ▲ p'_r) (········ and ■ p'_θ) at a) $y^+ = 4$, b) $y^+ = 10$, c) $y^+ = 50$, d) $y^+ = 120$; lines $N = 0$, symbols $N = 2$.
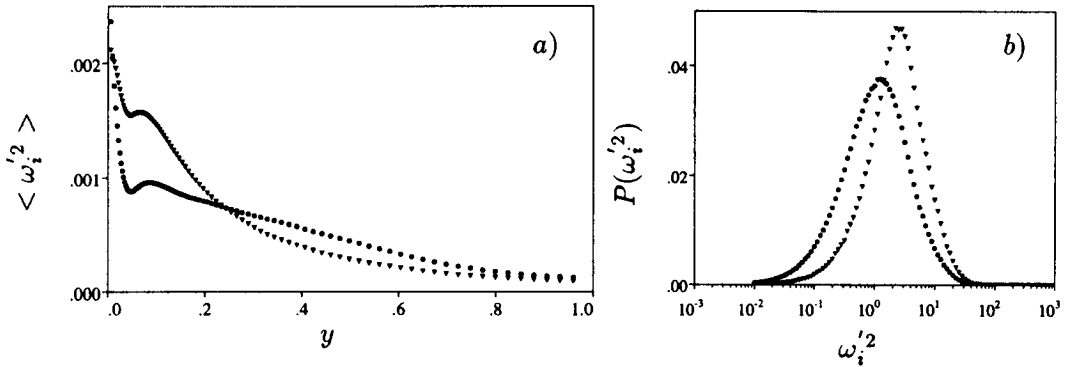
FIGURE 6. a) Dissipation radial profile, b) Probability density function of the local dissipation at $y^+ = 10$; $\triangle$ $N = 0$, $\bullet$ $N = 2$.

having positive rather than negative values of p'_i. This occurrence is related to the high correlation of negative azimuthal gradients of axial velocity (negative tilting rotation) with positive v'_r and the high correlation of events with same sign of v'_r and ω'_θ. Fig. 5c also shows that in the non-rotating case positive and negative correlations for the azimuthal components of $\mathbf{v}' \times \boldsymbol{\omega}'$ are equally distributed. When the rotation is imposed the tendency towards the symmetry for the axial component occurs, in agreement with the decrease of difference between the two terms in Fig. 4a. The rotation produces bigger changes in the θ component that goes from theoretical zero values to positive value as shown in Fig. 4b. Fig. 5c emphasizes that the positive values are given by the major number of points where v'_r and ω'_x have equal sign. Ejections of fluid from the wall ($v'_r < 0$ in this case) are thus correlated with clockwise axial fluctuating vorticity. As mentioned above $< v'_x\omega'_r > - < v'_r\omega'_x >$, although it is of the same order as the axial component when $N = 2$, it gives a much smaller contribution to the energy production because it is multiplied by U_θ.

The local energy dissipation can be related to the helicity density in the sense that where there is an elevated helicity density the dissipation is reduced; thus we expect that since in the rotating pipe the helicity density increases the dissipation diminishes. In fact, Fig. 6a shows that in the wall region, mainly around $y^+ = 10$, there is a large reduction when the rotation is imposed. At $y^+ = 10$ the *pdf* of the dissipation $\epsilon' \approx \omega'^2_l$ in Fig. 6b shows that for $N = 0$ the maximum is shifted towards higher values and that the distribution is more peaked than for $N = 2$. The joint probability density distribution between local dissipation and helicity density was calculated and, as shown in Fig. 7a in the non-rotating case, the high levels of dissipation are correlated to low levels of h'. On the contrary, when the pipe rotates, Fig. 7b shows that the dissipation is reduced, increasing the probability of low dissipation and positive helicity density.

3. Conclusions

In this paper, the direct simulation of a turbulent pipe has been used to investigate how the turbulence production and dissipation change when a solid body rotation
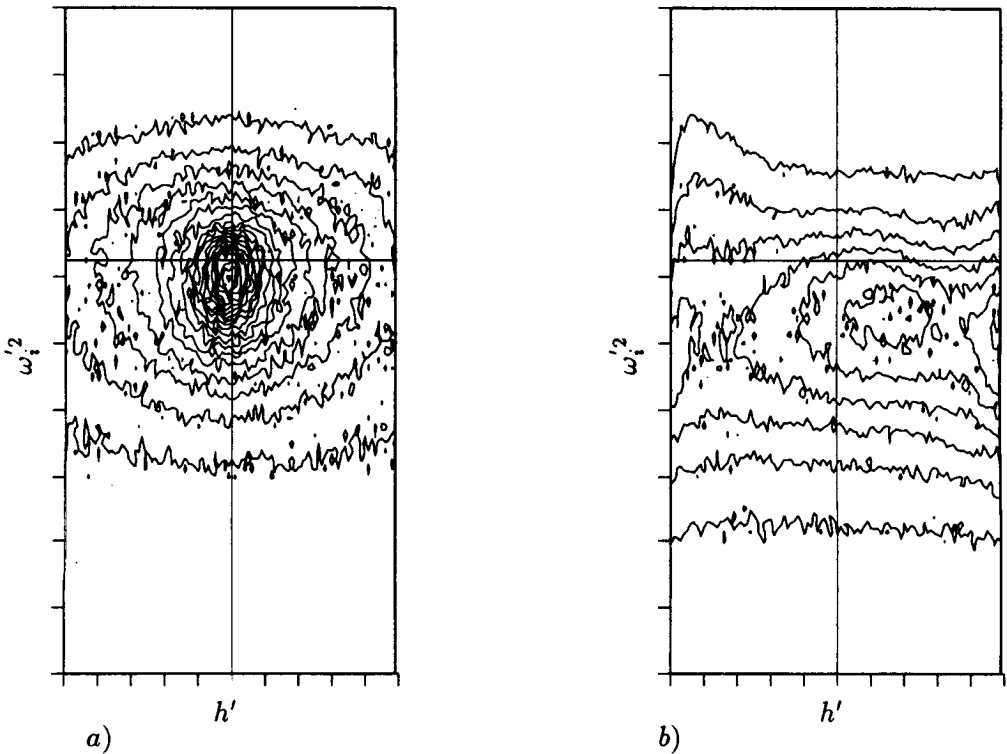
FIGURE 7. The joint *pdf* $P(\omega_i'^2, h')$ at $y^+ = 10$ for a) $N = 0$, b) $N = 2$. The horizontal scale goes from -1 to 1. The vertical scales goes from 10^{-2} to 10^{+2}. Two marks are separated by $10^{0.4}$.

is applied. The effect of background rotation on turbulent flows has a wide range of applications related e.g. to sound level reduction or combustion control and deserves further study. The pipe rotating about its axis is a very interesting case since the background rotation is parallel to the direction of the secondary vortical structures that play a fundamental role on wall friction and turbulence production. The global results of the imposed rotation on the turbulent pipe is drag reduction and a reduction of the turbulent kinetic energy near the wall. In the past, several studies were devoted to understanding whether the helicity density could be an indicator of dissipation levels. In the previous studies flows with zero mean helicity were considered, whereas in the rotating pipe the symmetry is disrupted by the rotation and a mean helicity is present. This study has shown that when the helicity increases, the dissipation is reduced. As a conclusion, which could be useful to achieve drag reduction, it can be asserted that to have a drag reduction the external action should be such as to disrupt the symmetry of right- and left-handed helical structures. It would then be interesting to use the direct simulation of three-dimensional boundary layers (Sendstadt & Moin 1991) to investigate whether this condition is verified. Of more practical interest will be to verify this occurrence in turbulent flows over riblets or dilute polymers solutions where a higher drag

reduction is achieved.

In this study the Navier Stokes equations in rotational form permit the turbulent energy production to be split into a part related to the energy cascade from large to small scales and into a part related to the convection by large scales. The full simulation data have shown the latter is greater than the former in the wall region and that, on the contrary, these two terms balance each other in the central region. From the *pdf* of the former, it has been shown how the vortical structures are changed in the wall region by the background rotation and how they are related to the changes in the energy production.

4. Future plans

The current study is limited to intermediate rotation rates $N \leq 2$. Of greater interest will be the increase in the rotation rate to reach the condition of complete laminarization. In this case, according to the Taylor-Proudman theorem, it is necessary to perform the simulations on a very long pipe, which would require a large number of grid points in the axial direction. This study is affordable and it will be done in the near future, using a parallel version of the code developed by our group in Rome that can run efficiently on parallel computers.

Acknowledgments

REFERENCES

BARDINA, J., FERZIGER, J. H. & ROGALLO, R. S. 1985 Effect of rotation on isotropic turbulence, Computation and modelling. *J. Fluid Mech.* **154.**

CHOI, H. & MOIN, P. 1994 Effects of the computational time step on numerical solutions of turbulent flow. *J. of Comp. Phys.* **113,** 1-4.

EGGELS, J. G. M., UNGER, F., WEISS, M. H., WESTERWEEL, J., ADRIAN, R. J., FRIEDRICH, R. & NIEUWSTADT, F. T. M. 1994 Fully developed turbulent pipe flow: a comparison between direct numerical simulation and experiment. *J.Fluid Mech.* **268,** 175-209.

HUSSAIN, A. K. M. F. 1986 Coherent structures and turbulence. *J. Fluid Mech.* **173,** 303-356.

KIM, J. 1939 The effect of rotation on turbulence structure. *Proc. 4th Intl. Symp. on Turb. Flows, U. Karlsruhe.* (6.1-6.4.)

KIM, J., MOIN, P. & MOSER, R. 1987 Turbulence statistics in fully developed channel flow at low Reynolds number. *J. Fluid Mech.* **177,** 133-166.

METAIS, O., FLORES, C., YANASE, S., RILEY, J. J., & LESIEUR, M. 1995 Rotating free-shear flows. Part.2 Numerical simulations. *J. Fluid Mech.* **293,** 47-80.

NISHIBORI, K., KIKUYAMA, K., & MURAKAMI, M. 1987 Laminarization of turbulent flow in the inlet region of an axially rotating pipe. *JSME International Journal.* **30,** 255-262.

ORLANDI, P. & FATICA, M. 1995 Direct simulations of a turbulent pipe rotating along the axis. *Submitted to J. Fluid Mech.*

PELTZ, R. B., YAKHOT, V., ORSZAG, S. A., SHTILMAN, L. & LEVICH, E. 1985 Velocity-vorticity patterns in turbulent flows. *Phy. Rev. Lett..* **54,** 2505-2508.

REICH, G. & BEER, H. 1989 Fluid flow and heat transfer in axially rotating pipe 1. Effect of rotation on turbulent pipe flow. *Int. J. Heat Mass Transfer.* **32,** 551-561.

ROGERS, M. M., & MOIN, P. 1987 Helicity fluctuation in incompressible turbulent flows. *Phys. Fluids.* **30,** 2662-2671.

SENDSTAD, O. & MOIN P. 1991 On the mechanism of 3-D turbulent boundary layers. *8th Symposium on turbulent shear flows, Munich 20-3.*

TSINOBER, A., EGGELS, J. G. M., & NIEUWSTADT, F. T. M. 1995 On alignments and small scale structures in turbulent pipe flow. *Fluid Dynamics Research.* **16,** 297-310.